HAL open science

Spin dependent electrochemistry and electrochemical enantioselective recognition with chiral methylated bis(ethylenedithio)-tetrathiafulvalenes

Andrea Stefani, Alexandra Bogdan, Flavia Pop, Francesco Tassinari, Luca Pasquali, Claudio Fontanesi, Narcis Avarvari

To cite this version:

Andrea Stefani, Alexandra Bogdan, Flavia Pop, Francesco Tassinari, Luca Pasquali, et al.. Spin dependent electrochemistry and electrochemical enantioselective recognition with chiral methylated bis(ethylenedithio)-tetrathiafulvalenes. The Journal of Chemical Physics, 2023, 159 (20), 10.1063/5.0171831 . hal-04456027

HAL Id: hal-04456027

https://univ-angers.hal.science/hal-04456027v1

Submitted on 13 Feb 2024

HAL is a multi-disciplinary open access archive for the deposit and dissemination of scientific research documents, whether they are published or not. The documents may come from teaching and research institutions in France or abroad, or from public or private research centers.

L'archive ouverte pluridisciplinaire **HAL**, est destinée au dépôt et à la diffusion de documents scientifiques de niveau recherche, publiés ou non, émanant des établissements d'enseignement et de recherche français ou étrangers, des laboratoires publics ou privés.

Spin dependent electrochemistry and electrochemical enantioselective recognition with chiral methylated bis(ethylenedithio)-tetrathiafulvalenes

Andrea Stefani,[1] Alexandra Bogdan,[2,3] Flavia Pop,[2] Francesco Tassinari,[4] Luca Pasquali,[5,6,7] Claudio Fontanesi,[5,a)], and Narcis Avarvari[2,a)]

[1]*Department of Physics, (FIM), Univ. of Modena, Via Campi 213/A, 41125 Modena, Italy.*

[2]*Univ Angers, CNRS, MOLTECH-Anjou, SFR MATRIX, F-49000 Angers, France.*

[3]*Babes-Bolyai University, Faculty of Chemistry and Chemical Engineering, Department of Chemistry and SOOMCC, Cluj-Napoca, 11 Arany Janos Str, 400028,Cluj-Napoca, Romania.*

[4]*Department of Chemical and Earth Science, (DSCG), Univ. of Modena, Via Campi 103, 41125 Modena, Italy.*

[5]*Department of Engineering "Enzo Ferrari", (DIEF), Univ. of Modena, Via Vivarelli 10, 41125 Modena, Italy.*

[6]*IOM-CNR, Strada Statale 14, Km. 163.5 in AREA Science Park, Basovizza, 34149 Trieste, Italy.*

[7]*Department of Physics, University of Johannesburg, P.O. Box 524, Auckland Park 2006, South Africa.*

[a)]Authors to whom correspondence should be addressed: claudio.fontanesi@unimore.it and narcis.avarvari@univ-angers.fr

ABSTRACT

Enantio-discrimination and spin-dependent electrochemistry (SDE), as a manifestation of the chirality induced spin selectivity (CISS) effect, are important phenomena that can be probed by "chiral" electrochemistry. Here we prepared chiralized surfaces of gold and nickel, to serve as working electrodes, through effective chemisorption of enantiopure dimethyl-bis(ethylenedithio)-tetrathiafulvalene (DM-BEDT-TTF) **1**, tetramethyl-bis(ethylenedithio)-tetrathiafulvalene (TM-BEDT-TTF) **2** and of their capped silver nanoparticles (AgNPs) aggregates by simple incubation of the metallic substrates. The effective chemisorption was checked by means of ultra-high vacuum (UHV) X-ray photo electron spectroscopy (XPS) and by electro-desorption experiments, i.e. cyclic voltammetry (CV) scans showing a first electro-desorption peak at about -1.0 V. The Au|**1** and Au|**2** chiral electrodes were successfully used in CV experiments exploiting chiral redox probes. Finally, the hybrid interfaces Ni|enantiopure **1** or **2**|AgNPs served as working electrodes in SDE experiments. In particular, the hybrid chiral interfaces Ni|(*R*)-**2**|AgNPs and Ni|(*S*)-**2**|AgNPs exhibited a significant

spin-filtering ability, as a manifestation of the CISS effect, with average spin polarization values of 15%.

I. INTRODUCTION

One of the most exciting properties of chiral molecules and materials, which currently triggers a massive interest in chemistry, physics and biology, is the electron spin selective transmission referred to as chirality induced spin selectivity (CISS) effect.[1,2] Accordingly, in a simplified model, an electron of up spin traverses a homochiral medium more easily than the down spin, the situation being reversed for the opposite handedness of the molecule.[3] The CISS effect stems from the experimental observation that charge transmission through enantiopure chiral interfaces is spin-selective. As a result, the current flowing through an enantiopure system is spin-polarized. It has been shown that this phenomenon can have huge interest, among others, in quantum technologies,[4] enantioselective chemistry,[5] enantiomer separation[6] or water splitting.[7,8,9] Since the pioneering results of Naaman *et al.* on the exceptional high spin polarization values reached with double-stranded DNA self-assembled monolayers on gold in low-energy photoelectron transmission experiments,[10] several CISS active systems have been described,[11,12,13] including small chiral molecules such as helicenes deposited on metallic surfaces[9,14] or on highly oriented pyrolytic graphite (HOPG).[15] One of the manifestation of the CISS effect is through the spin dependent electrochemistry (SDE) paradigm, where the charge transmission is determined *via* electrochemical methods. Typically, cyclic voltammetry (CV) measurements as a function of spin-injection from a ferromagnetic chirally functionalized electrode show current intensity depending on the magnetization of the electrode relative to the chirality of the adsorbed compound.[16,17,18] Thus, several chiral substrates such as the transmembrane protein bacteriorhodopsin (bR),[19] helical oligopeptides[20] or double-stranded DNA[21] in the presence of the $K_4[Fe(CN)_6]/K_3[Fe(CN)_6]$ bulk redox couple, chiral conductive polymers in the presence of Fc/Fc^+ (Fc = ferrocene),[22] or L- or D- cysteine molecule (either L or D) covalently functionalized by the redox probe toluidine blue O (TBO)[23] have been deposited on Ni or Ni/Au surfaces which served as working electrodes. Values of the spin polarization (SP), defined as $SP = I_\uparrow - I_\downarrow / I_\uparrow + I_\downarrow$, where $I_\uparrow$ and $I_\downarrow$ represent the current when the nickel electrode is magnetized up or down by an external permanent magnet, generally ranging between 5 and 20% have been measured. Note that in the case of the helical conducting polymers SP reached up to 34 – 50% at short times after the voltage pulse (2 – 3 s) and drastically decreased at longer times, possibly as a consequence of changes in the polymer conformation under the influence of the applied electric field.[22] These polymers were actually polythiophenes and they were very likely adsorbed on the Ni/Au electrode thanks to the

favorable Au···S interactions. It is therefore interesting to use sulfur containing chiral compounds to coat the surface of this type of magnetic electrodes.

Besides the CISS effect through the spin-dependent electrochemistry, another direct application of chirally functionalized electrodes is the possibility to electrochemically address the enantiomer discrimination of a chiral analyte, a field of investigation which is continuously increasing as well.[24,25] Indeed, electron transfer processes taking place at enantiopure chiral interphases translate into different potentials for the two enantiomers of a chiral probe in voltammetric measurements.[26] Moreover, the enantiomer concentration and even an estimation of the enantiomeric excess can be determined from the relation between concentration and current intensity.

Certainly, the most important family of sulfur rich electroactive molecular precursors for chiral crystalline conductors is that of chiral tetrathiafulvalenes (TTF),[27] which considerably developed within the last decade,[28] very much motivated by the observation of direct or indirect chirality triggered effects in the electrical conductivity, such as the electrical magnetochiral anisotropy (eMChA) effect[29] for the former or the modulation of the crystalline packing for the latter.[30,31,32] Some of the most popular chiral TTFs are the methylated BEDT-TTF [BEDT = bis(ethylenedithio)] derivatives, such as DM-BEDT-TTF (DM = dimethyl) **1**[33] and TM-BEDT-TTF (TM = tetramethyl) **2**,[34,35] which provided important series of chiral conductors with peculiar properties and structures,[36,37,38,39,40] not encountered in the achiral homologue BEDT-TTF (Fig. 1).

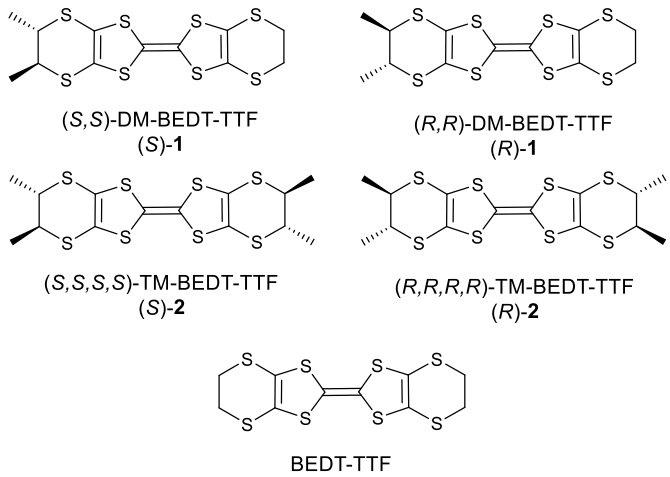

FIG. 1. Chiral TTF derivatives **1** and **2** investigated in this work for SDE and their achiral homologue BEDT-TTF.

However, neither CISS investigations nor electrochemical enantio-discrimination have been reported so far with chiral TTF precursors, despite of the propensity of TTF to self-assemble on Au surfaces.[41] We report herein spin-dependent electrochemistry (SDE), as a consequence of the CISS effect, and chiral electrochemical recognition with the chiral BEDT-TTF derivatives **1** and **2**.

II. EXPERIMENTAL

A. Materials

Sodium nitrate $NaNO_3 \geq 99.0\%$, KCl ≥ 99.0%, ferrocyanide $K_4[Fe(CN)_6]$, ferricyanide $K_3[Fe(CN)_6]$ are from Sigma Aldrich and were used without further purification. Ethanol $C_2H_6O \geq 99.5\%$ from Merck was used without further purification. 3,4-Dihydroxy-L-phenylalanine (referred as L-DOPA in the text), (*S*)-(-)-N,N-dimethyl-1-ferrocenylethylamine 98% (referred as S-FC in the text), (*R*)-(+)-N,N-dimethyl-1-ferrocenylethylamine 97% (referred as R-FC in the text) are from Alfa Aesar and were used without further purification. A ferrocyanide 5 mM / ferricyanide 5 mM in a KCl 0.1 M aqueous solution is referred as the Fe(III)|Fe(II) redox couple in the text. DM-BEDT-TTF **1** and TM-BEDT-TTF **2** were prepared according to the published protocols.[33,34]

A.1 Gold functionalization

Au(111)-oriented surfaces were obtained by e-beam evaporation of 100 nm of gold, on a silicon substrate (Siltronix), with thermally grown 300 nm SiO_2 (100), > 400 Ω cm, on an 8-nm-thick Cr adhesion layer, followed by gentle flame annealing just prior to use (in the following Au stays for Au(111)-oriented). Gold functionalization is obtained by 24 hours incubation of the Au surface in a 5 mM TTF-derivative solution in ethanol.

A.2 Silver nanoparticles preparation

AgNPs are obtained exploiting the electrochemical based method of Starowicz et al.,[42] obtaining AgNPs with dimension ranging between 20 and 50 nm.[43]

A.3 TTF-derivative capped AgNPs preparation [(*S*)-1@AgNPs, (*R*)-1@AgNPs, (*S*)-2@AgNPs and (*R*)-2@AgNPs)]

The electrochemically fabricated AgNPs (*vide supra*, section A.2) were added to a 5 mM TTF-derivative ethanolic solution in order to obtain TTF capped-silver nanoparticles ((*S*)-**2**@AgNPs for example). The solution was left at rest under dark for 24 hours at room temperature. Then, the resulting pale-yellow solution (free of visible precipitate to the naked eye) was subjected to centrifugation at 6000 rpm for 30 minutes, followed by decantation of the supernatant and replacement with fresh solvent. This cycle is repeated twice to purify the AgNPs@TTF-derivatives from excess, non-adsorbed molecules.

A.4 Nickel functionalization

Ni surfaces were obtained by e-beam evaporation of 100 nm of nickel, on a silicon substrate (Siltronix) with thermally grown 300 nm SiO_2 (100), > 400 Ω cm, on an 8-nm-thick Ti adhesion layer.

A one-step Ni-functionalized preparation strategy was followed. Ni functionalized surfaces were obtained by immersion in a suspension of TTF-derivative capped Ag nanoparticles (yielding a hybrid Ni|(*S*)-**1**@AgNPs chiral interface and so on). During the functionalization process the Ni surface was kept at a negative (reducing) potential of -0.3 V, to avoid nickel oxidation.

B. Electrochemical set-up

Electrochemical measurements were performed using an Autolab PGSTAT 128N and CH-Instruments CHI660A potentiostats. A typical three-electrode cell is employed: a Pt sheet and a silver, silver chloride, KCl saturated solution ($Ag/AgCl/KCl_{sat}$) electrodes were the counter and reference electrodes, respectively. Evaporated gold substrates served as the working electrode (WE): 100 nm gold (Lesker) was evaporated on top of a 10 nm Ti layer on SiO_2 (100) wafer (Siltronix) and then followed by gentle flame annealing to obtain Au(quasi-111). 0.1 M KCl and K_2SO_4 aqueous solution were used as base electrolyte. All the potentials reported in this work are referred to the $Ag/AgCl/KCl_{sat}$ reference electrode.

C. UHV surface characterization

X-ray photoemission spectroscopy measurements (XPS) were carried out employing a MgKα source. The electron analyzer was an Omicron EA125, installed at LFMS lab, Department of Engineering Enzo Ferrari, University of Modena, Italy. Photoemission measurements were carried out at normal emission with a resolution of 0.5 eV. The S 2p XPS spectra have been fitted, after a Shirley background subtraction, using Voigt doublet functions accounting for the spin-orbit splitting of 1.2 eV between S $2p_{3/2}$ and S $2p_{1/2}$ components. The measurements were performed at room temperature. Binding energies are referred to the Fermi energy of a gold substrate.

III. RESULTS AND DISCUSSION

A. Au electro-desorption experiments

Figure 2 shows CVs relevant to the electro-desorption experiments of enantiopure (*S*)-**1** and (*S*)-**2** SAMs chemisorbed on Au, after overnight incubation in ethanol solution. CVs were recorded in a 5 mM Fe(III)|Fe(II), 0.1 M KCl aqueous solution, Fig. 2(a) black line shows the reference CV recorded on a bare and freshly cleaned gold surface, the red line curve is the CV recorded on the Au functionalized with (*S*)-**2**; please note the substantial decrease in the current and the absence of neat peaks, replaced by two “shoulders” featuring a potential difference of about 300 mV. Fig. 2(b) shows the electro-desorption CVs for the Au/(*S*)-**2** interface, which acts as the WE: the first two scans are carried out in the -0.1 to 0.5 V potential window (red line) then the potential scan window is widened

to -1.6 V (black line). In the first scan in the negative potential range two peaks (reduction current, negative in sign) are evident in the -1.0 to -1.4 V potential range (labelled as E_{des1}); in the following potential scans the current is definitively lower showing a much weaker peak at -1.0 V (labelled E_{des2}). Figs. 2(c) and 2(d) show exactly the same type of experiment carried out for the Au functionalized with (*S*)-**1**. The blue curves in Figs. 2(c) and 2(d) refer to the functionalized surface, for which a similar behavior is observed compared to Figs. 2(a) and 2(b), excepting the E_{des1} pattern. Indeed, the latter is much more neat and defined with respect to the result observed for (*S*)-**2**. Thus, the SAM formed by (*S*)-**1** is very likely a little more ordered with respect to the SAM formed by (*S*)-**2**. In addition, the charge calculated by integration of the E_{des1} peaks yields a surface area of 0.55 and 0.80 nm^2 for the SAMs of **1** and **2**, respectively, suggesting an orientation of **1** a little more tilted with respect to the electrode surface, while **2** should be adsorbed almost "flat" on the surface. Indeed, the latter values of surface coverage match reasonably well with the theoretical projected area of (*S*)-**1** and (*S*)-**2** disposed almost flat on the electrode surface, the calculations of the surface having been performed by using the Van der Waals radii (see the SI).

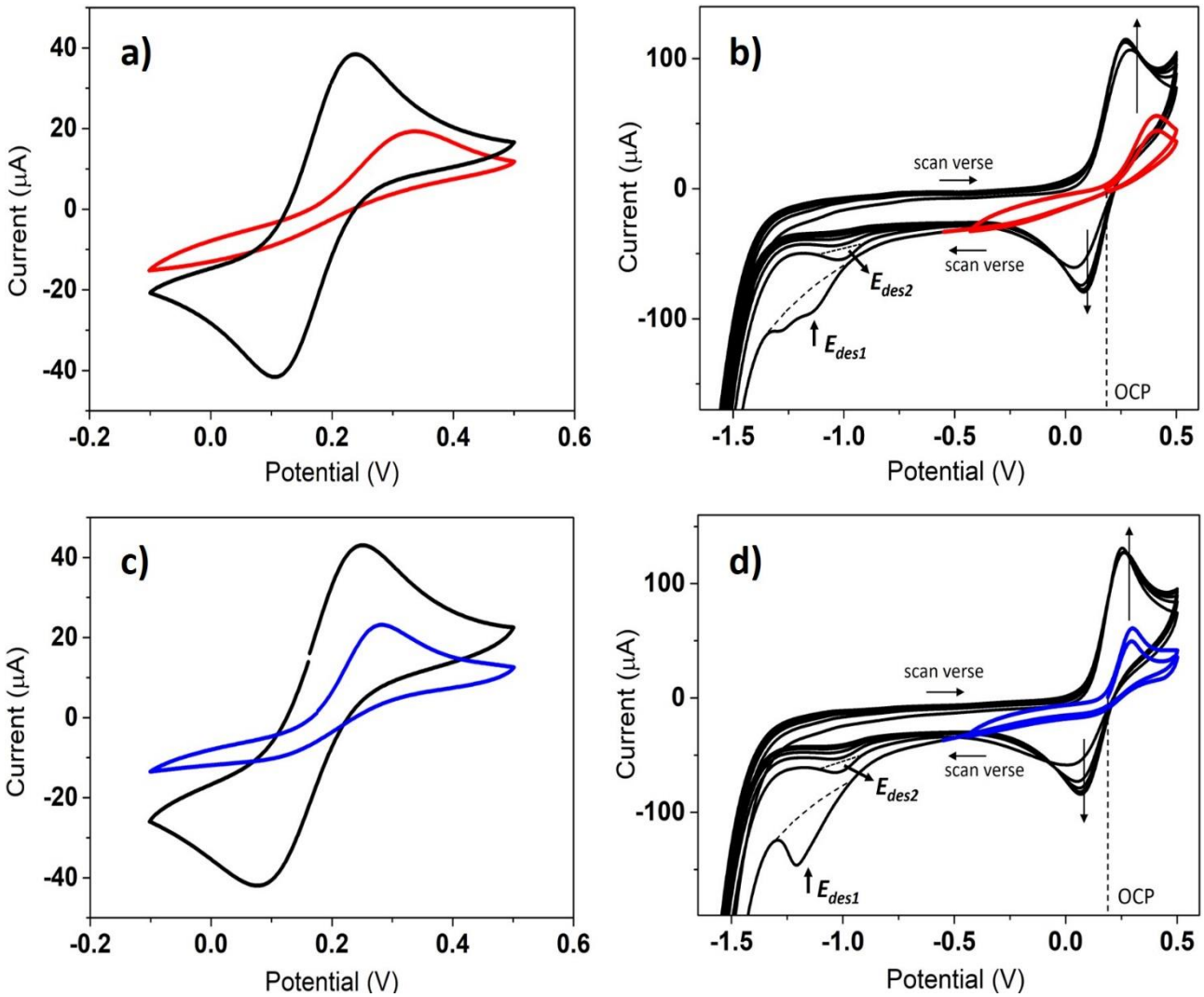

FIG. 2. CV curves of a 5 mM Fe(III)|Fe(II), 0.1 M KCl aqueous solution, recorded at the Au|(*S*)-**2** (a and b panels) and

at the Au|(*S*)-**1** (c and d panels) and d)) in a three-electrodes electrochemical cell (Ag/AgCl is the Ref, a Pt sheet the Counter Electrode). (a) 0.1 V s^{-1} potential scan rate: the red line is the Au|(*S*)-**2** interface acting as the WE, the black line is the same Au|(*S*)-**2** WE after the electro-desorption procedure; (b) 0.5 V s^{-1} potential scan rate: the red line is the CV forward 2 scans recorded before electro-desorption, the black curves feature a main peak (labelled as E_{des1} in Fig. 2b) in the first reductive scan and a small peak (E_{des2}) in the second scan (due to the electro-desorption of (*S*)-**2**): the first CV forward scan starts from OCP to 0.5 V, then the potential is scanned from 0.5 to -1.7 V; the successive 6 CV scans are carried out in the -1.7 to 0.5 V potential range; (c) 0.1 V s^{-1} potential scan rate: the blue line is the Au|(*S*)-**1** interface acting as the WE, the black line is the same Au|(*S*)-**1** WE after the electro-desorption procedure; (d) 0.5 V s^{-1} potential scan rate: the blue line is the CV forward 2 scans recorded before electro-desorption, the black curves feature a main peak (labelled as E_{des1} in Fig. 4d) in the first reductive scan and a small peak (E_{des2}) in the second scan (due to the electro-desorption of (*S*)-**1**): the first CV forward scan starts from OCP to 0.5 V, then the potential is scanned from 0.5 to -1.7 V; the successive 6 CV scans are carried out in the -1.7 to 0.5 V potential range.

B. XPS analysis

Fig. 3 shows the S2p XPS spectra relevant to the Au, Ni and Ag surfaces functionalized with the **1** and **2** SAMs: red dots are the experimental data, blue thick line the overall fit of the experimental curve, thin lines represent single Voigt doublets. Au and Ni functionalized surfaces have been produced by incubation of clean surfaces in solution (details of the functionalization procedure are reported above in section IIA), whilst functionalized Ag nanoparticles have been directly dropcasted on a clean glassy carbon flat surface.

Figs. 3(a) and 3(b) show XPS S 2p spectra for the Au|(*R*)-**1** and Au|(*R*)-**2** interfaces. The peak in the 166 to 160 eV range can be effectively fitted by two main components centered at 164.1 (due to the free, not chemically-bound sulfur) and 162.2 eV (associated to S atoms chemisorbed onto the Au surface[44,45,46,47,48,49]). The absence of any signal for energy values larger than 166.5 eV further supports the effective gold surface functionalization (signals at energies larger than 166.5 eV are typical of oxidized sulfur).[50,51] All in all, XPS results concerning the Au|(*R*)-**1** and Au|(*R*)-**2** interfaces suggest bonding between the metal and the chiral molecules.

Figs. 3(c) and 3(d) show XPS S 2p spectra for the Ni|(*R*)-**1** and Ni|(*R*)-**2** interfaces, a rather neat difference being observed between them. Spectra in Figs. 3(c) and 3(d) feature a prominent peak at 164 eV which has the typical line-shape of thiophene-based SAMs. Both interfaces present the two components related to bound and free thia-heterocycles, with Ni|(*R*)-**2** showing a slightly larger chemisorbed/unbound component ratio with respect to Ni|(*R*)-**1**, suggesting a stronger bonding for Ni|(*R*)-**2**. Also, a prominent component is found for Ni|(*R*)-**1** at binding energies larger 166.5 eV, indicating a not negligible amount of oxidized sulfur, whilst for the Ni|(*R*)-**2** interface this peak is significantly smaller.

Figs. 3(e) and 3(f) show XPS S 2p spectra for the Ag|(*R*)-**1** and Ag|(*R*)-**2** interfaces. All in all the outcome of the XPS spectra parallel the results obtained for the Ni interface, with a slightly larger

oxidized sulfur contribution for the Ag|(*R*)-**1** interface with respect to the Ag|(*R*)-**2** one, and a larger contribution from bounded sulfur for the Ag|(*R*)-**2** system, in any case giving strong evidence for the effective AgNPs capping by the chiral TTFs **1** and **2**.

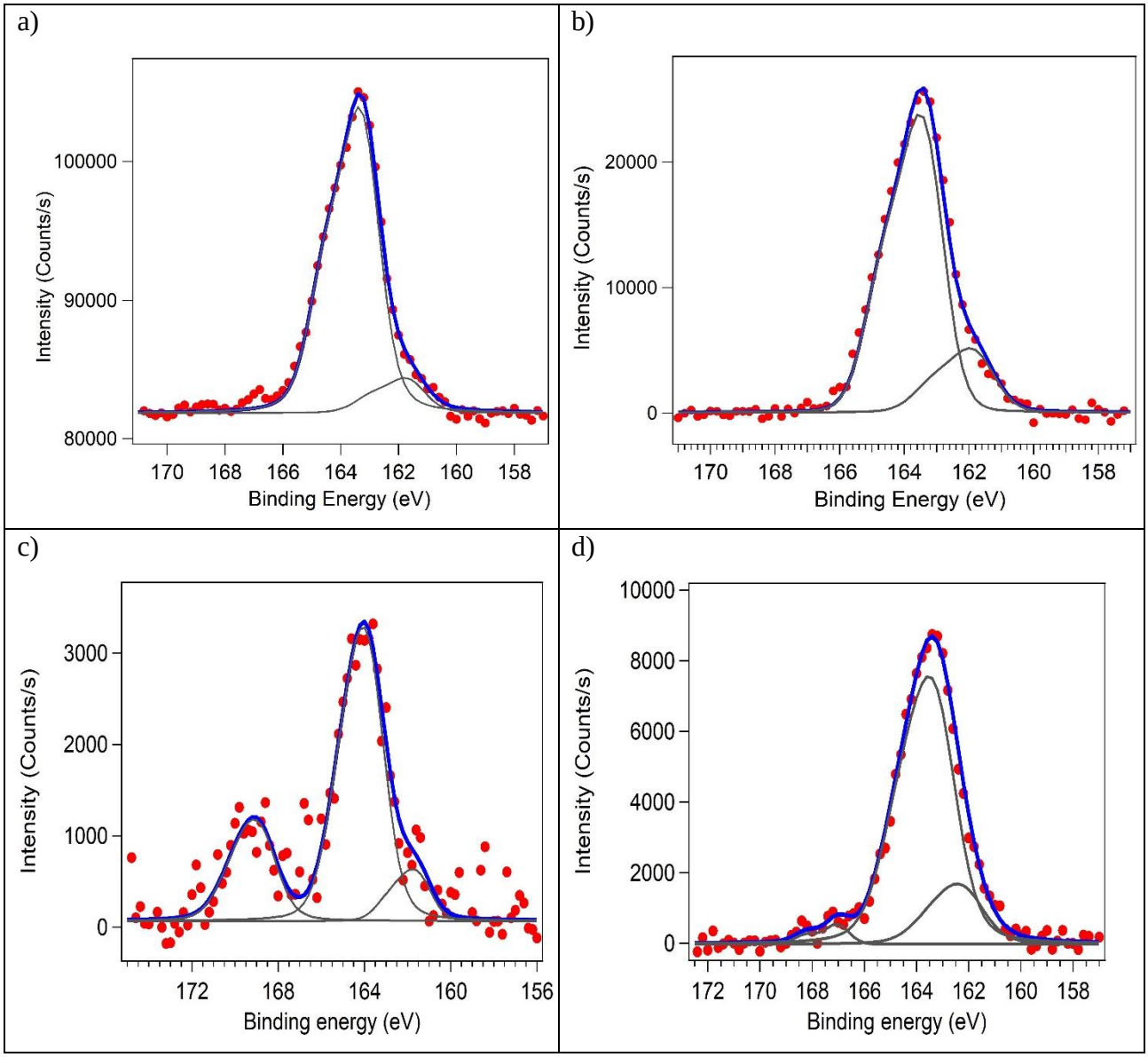

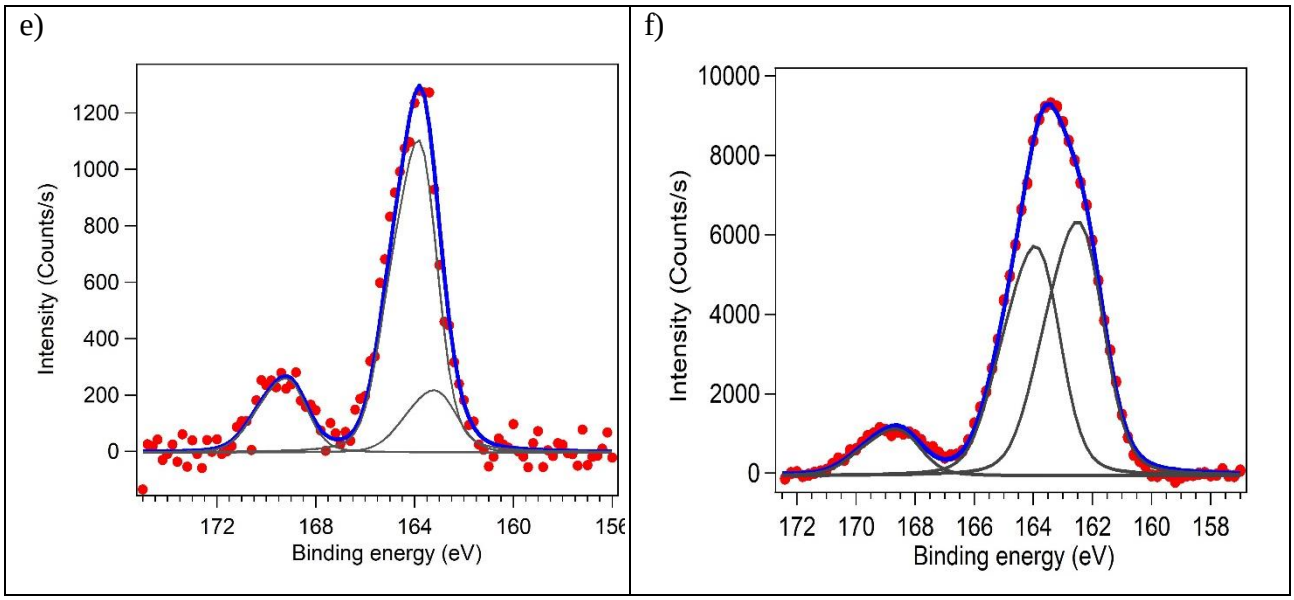

FIG. 3. S 2p core-level XPS spectra, Mg Kα photons, 1.254 keV photon energy. (a) Au|(*R*)-**1** interface; (b) Au|(*R*)-**2** interface; (c) Ni|(*R*)-**1** interface; (d) Ni|(*R*)-**2** interface; (e) (*R*)-**1**@AgNPs suspension drop-casted on Glassy Carbon; (f) (*R*)-**2**@AgNPs suspension drop-casted on Glassy Carbon.

C. Enantio-recognition with the chiral gold electrodes

Electrochemical enantiomer discrimination in both analytical and preparative contexts is of great fundamental and applicative interest.[24,25] This technique most commonly involves the occurrence of a diastereomeric relation between a chirally modified electrode surface, serving as working electrode (WE), and a chiral analyte. Accordingly, chiral modifiers such as tartaric acid,[52] chiral PEDOT (poly-3,4-ethylenedioxythiophene) derivatives,[53] oligomers of the axially chiral 2,2'-bis[2-(5,2-bithienyl)]-3,3'-bi-thianaphthene (BT_2T_4),[54] Cu(II) cysteine complexes,[55] thiahelicenes,[56] have been deposited on Ni, Au or glassy carbon electrodes for the enantio-recognition of a large variety of analytes including the commercially available N,N-dimethyl-1-ferrocenylethylamine (S-FC and R-FC hereafter for the (*S*) and (*R*) enantiomers), provided with planar chirality thanks to the electroactive ferrocene unit, or the L-dopamine (L-Dopa hereafter).[56,57]

In the present work we have evaluated the enantio-discrimination ability of our Au/**1** and Au/**2** chiral interfaces as working electrodes (WE) towards N,N-dimethyl-1-ferrocenylethylamine and L-dopamine. As can be observed from Figs. 4(a), 4(b), 4(e) and 4(f) excellent enantio-recognition is obtained with S-FC and R-FC for both platforms, as evidenced by the large differences in the peak potential values, i.e. average values of 150 mV for the system Au/**1**//FC (compare Fig. 4(a) and 4(b)) and of 90 mV for the system Au/**2**//FC (compare Fig. 4(e) and 4(f)). It can be thus hypothesized that the interaction between the chiral TTFs **1**-**2** and FC involves the chiral group of the ferrocene unit, possibly through hydrogen bonding interactions that can establish between the NMe_2 group attached

to the stereogenic center of FC and H atoms of the ethylene groups.[58] Note that for both systems the oxidation of FC is perfectly reversible.

For comparison sake we report in Table 1 the peak potential values reported for closely related systems, i.e. Au, Ni or glassy carbon (GC) electrodes and various chiral analytes, including N,N-dimethyl-1-ferrocenylethylamine (FC) and L-Dopa as in the present study.

TABLE I. Average peak potential difference for the electrochemical enantio-recognition.

Reference	Working electrode (WE)	Chiral analyte	ΔE (mV)
[52]	Ni/tartaric acid	glucose	120
[53]	GC/PEDOT	Dopa	50
[54]	GC/oligo-(BT_2T_4)	ferrocenes	20 - 120
[56]	GC/[7]thiahelicene	FC	250
[56]	GC/[7]thiahelicene	Dopa	350
this work	Au/**1** and Au/**2**	FC	150 and 90
this work	Au/**1** and Au/**2**	Dopa	50 and 120

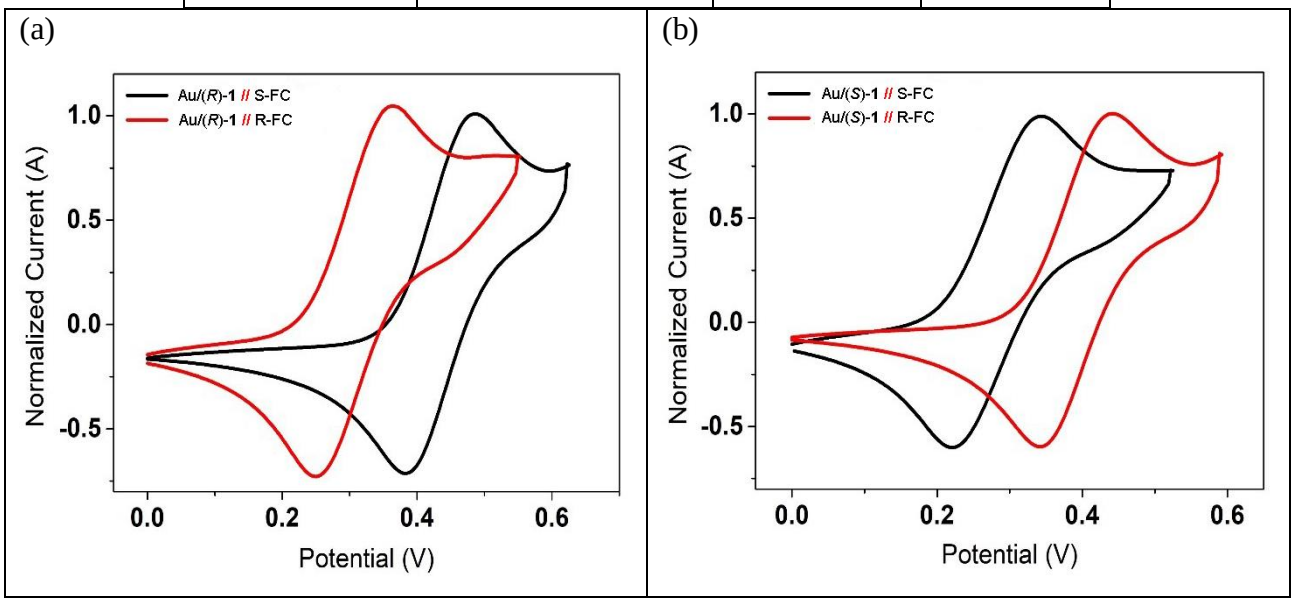

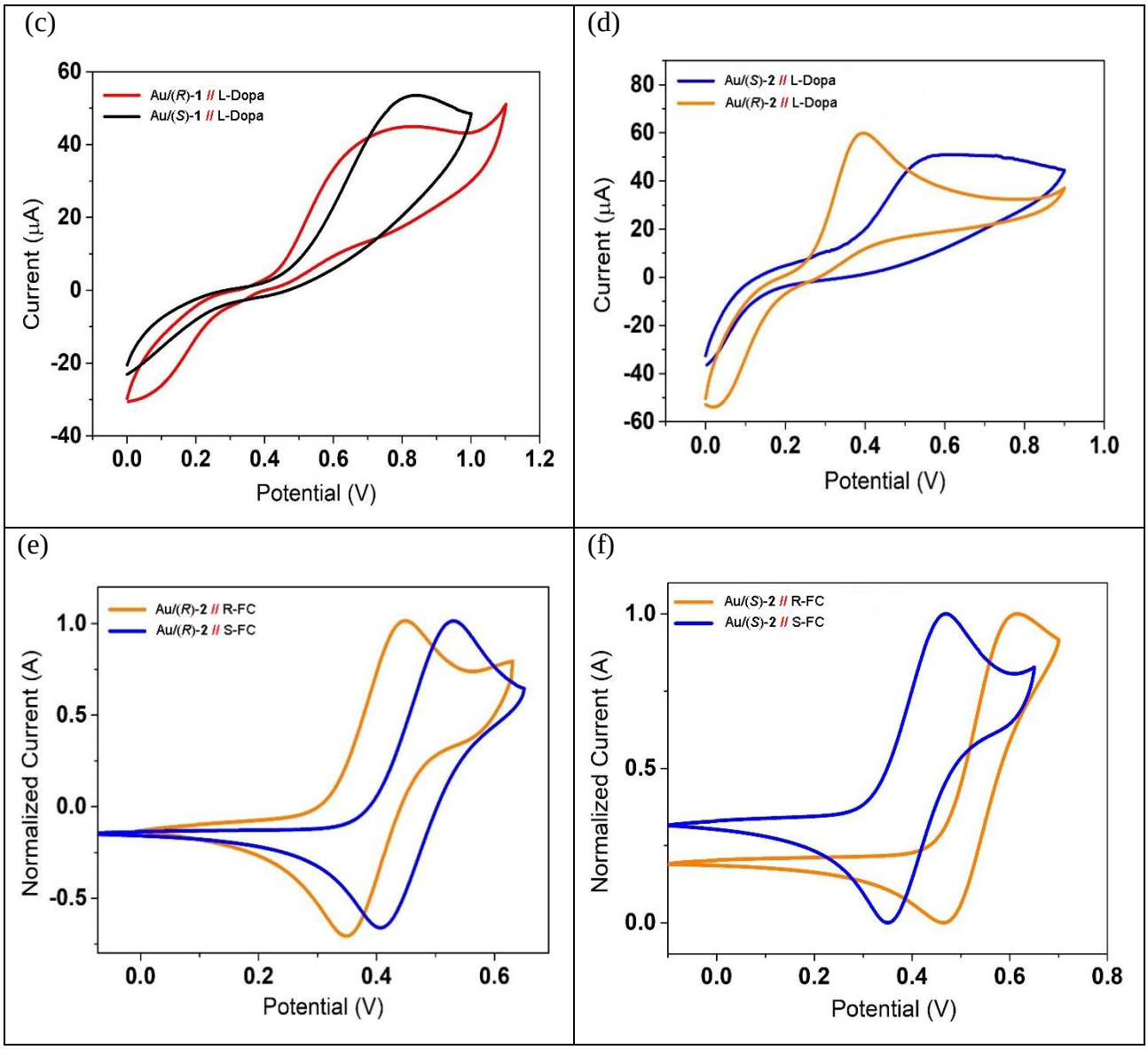

FIG. 4. Voltammetric measurement of the Au|(*R*)-**1** & Au|(*S*)-**1** interfaces (panels a, b, c) and of the Au|(*S*)-**2** & Au|(*R*)-**2** interfaces (panels d, e, f), acting as the WE. CVs were recorded with a 0.05 V s^{-1} potential scan rate and the support electrolyte is 0.1 M tetrabutylammonium tetrafluoroborate (TBATFB) in ACN solution. (a) CV curves in 5 mM S-FC (black curve) or R-FC (red curve); the WE is the Au|(*R*)-**1** interface; (b) CV curves in 5 mM S-FC (black curve) or R-FC (red curve); the WE is the Au|(*S*)-**1** interface; (c) CVs curves in 2 mM L-Dopa recorded at the Au|(*R*)-**1** (red curve) and at the Au|(*S*)-**1** interface (black curve); (d) CVs curves in 2 mM L-Dopa recorded at the Au|(*S*)-**2** (blue curve) and at the Au|(*R*)-**2** interface (orange curve); (e) CV curves in 5 mM R-FC (orange curve) or S-FC (blue curve); the WE is the Au|(*R*)-**2** interface; (f) CV curves in 5 mM S-FC (orange curve) or R-FC (blue curve); the WE is the Au|(*S*)-**2**.

The enantio-discrimination of our platforms with L-Dopa is comparatively less efficient, but still not negligible, as highlighted in Figs. 4(c) and 4(d). As usually observed for this analyte, its oxidation is irreversible,[56] therefore only the oxidation peak potentials are considered in order to determine the diastereomeric potential differences, which are just larger than 50 mV for Au/**1**/L-Dopa (compare Fig. 4(c), indeed referred to the onset potential, peaks are rather broad) and 120 mV for Au/**2**/L-Dopa (compare Fig. 4(d)) with an oxidation at lower potentials for the (*R*) enantiomers of **1** and **2**. Different competing intermolecular interactions could take place between L-Dopa and the TTFs **1** and **2**, such as: *i*) hydrogen bonding involving the H atoms of the ethylene bridges of **1** and **2**, as mentioned above,

and the *ortho*-dihydroxy group of L-Dopa, which would not provide an efficient discrimination as this group is remote from the stereogenic center, *ii*) π-π interactions between the two π frameworks, which would probably afford a better chiral recognition for **2** which possesses stereogenic centers on both sides of the π system, and, finally, *iii*) hydrogen bonding involving the chiral α-amino-acid group of L-Dopa and the H atoms of the TTF ethylene groups. All in all, the enantio-discrimination towards L-Dopa is more efficient for **2**, containing four stereogenic centers, than for **1**, with two stereogenic centers.

D. Spin dependent electrochemistry (SDE)

The ultimate goal of our investigations with the chiral TTF precursors **1** and **2** was the demonstration of the CISS effect through spin dependent electrochemistry experiments. To reach this goal, we have prepared ferromagnetic nickel electrodes coated with enantiopure **1** and **2**, according to previous reports on such chiral working electrodes.[19] Functionalized Ni/TTF@AgNPs surfaces were obtained by overnight incubation of the compounds **1** and **2** capped with AgNPs (see the section II.A.4). Although our chiral precursors are redox active themselves, their first oxidation potentials occur at 0.50-0.53 V *vs* SCE (saturated calomel electrode). Unfortunately, these oxidation values are more positive than the oxidation potential of the nickel surface. We have therefore decided to use as redox mediator AgNPs,[43] which oxidize at lower potential than Ni. Figures 5(a) and 5(b) show SDE results for surfaces chiralized with **1,** the results being consistent with swapping the spin-injection (i.e. flipping the magnet under the Ni WE). In Fig. 5(b), S-surface, the current is larger for the Mag DOWN disposition, while the opposite is found for the R-surface (Fig. 5(a)) in the reduction peak, but not in the oxidation current (see also the SI).

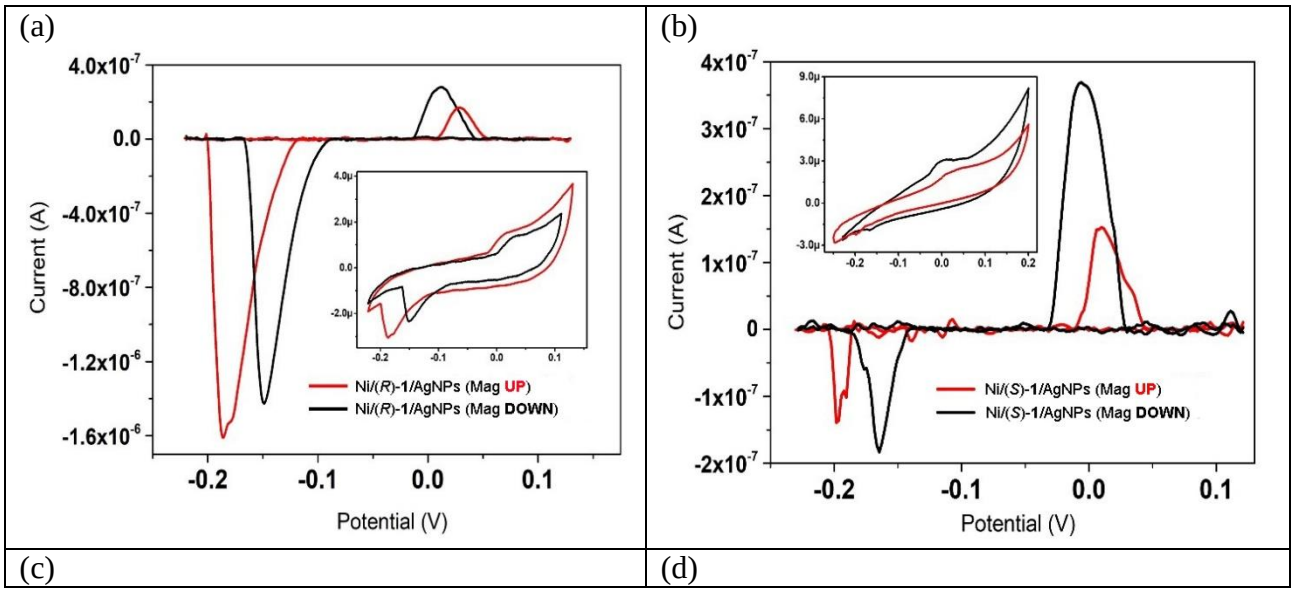

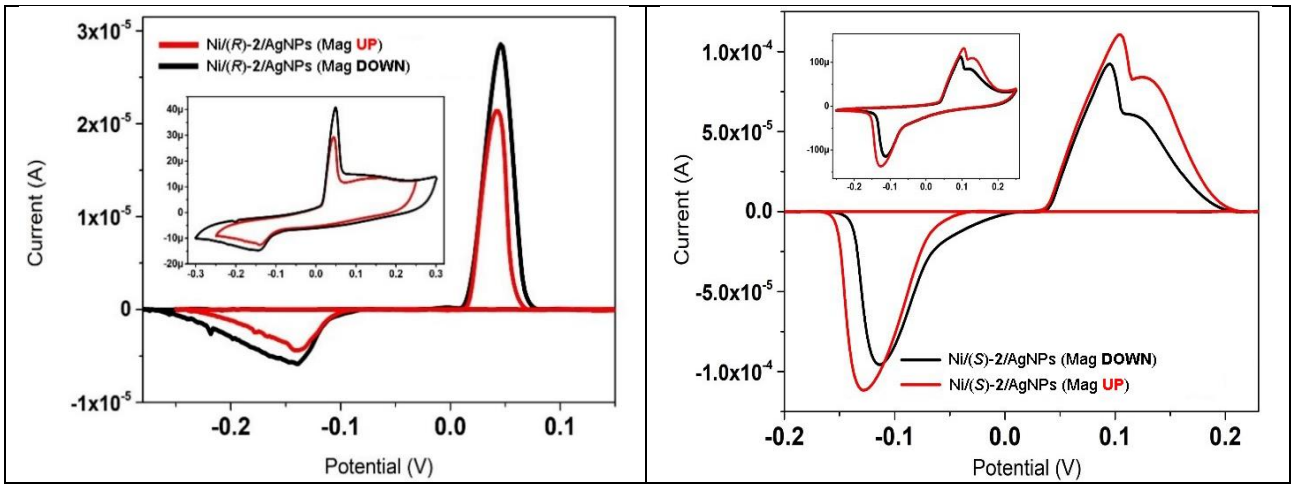

FIG. 5. Spin-dependent electrochemistry CVs: a Pt sheet and Ag/AgCl/KClsat are used as the CE and RE, respectively. CVs were recorded with a 0.05 V s^{-1} potential scan rate in a 0.1 M KCl aqueous solution. (a) Ni|(*R*)-**1**|AgNPs interface acts as WE; (b) Ni|(*S*)-**1**|AgNPs interface acts as WE; (c) Ni|(*R*)-**2**|AgNPs interface acts as WE; (d) Ni|(*S*)-**2**|AgNPs interface acts as WE. Black solid curve magnet DOWN orientation. Red solid curve magnet UP orientation. The main panels display the data after background subtraction (removal of the double layer contribution), while the insets show the raw data from the corresponding measurements.

The calculated spin polarization values are 6% for (*R*)-**1** and 13% for (*S*)-**1**, spin polarization being defined as:

$$SP\% = \frac{\left(I_{MagUP} - I_{MagDOWN}\right)}{\left(I_{MagUP} + I_{MagDOWN}\right)} \times 100 \qquad (1)$$

I_{MagUP} and $I_{MagDOWN}$ are the peak current values recorded with the magnet orientation UP and DOWN, respectively.

Figures 5(c) and 5(d), related to (*R*)-**2** and (*S*)-**2**, respectively, show much more consistent SDE behavior, i.e. the R-surface shows magnet DOWN spin selectivity, while the S-surface shows magnet UP spin selectivity, with spin polarization values on the average just below 15%, as calculated from the maximum value of current at the peaks in the cyclic voltammograms, which are values in the usual range observed for different combinations of chiral/redox couples (mediators) in the area of spin-dependent electrochemistry.[16–18] However, the present system is very easy to implement since the chiral mediator consists in the simplest chiral TTF precursors for which the synthesis is straightforward. Going into details: the SDE results for **2** compared to **1** appear a bit more robust (this at variance of enantio-recognition results, please compare Figure 4 CVs and the relevant discussion in section C). This could be most likely related to the different Ni-TTF interaction: spin-injection efficiency depends also on the reciprocal spatial disposition – geometry of adsorption on the electrode – of the chiral molecule on the electrode surface. Indeed, precursor **1** contains a more accessible side, without methyl substituents, which is prone to interact stronger with the surface (although possibly

leading to a twisted adsorbed disposition). In addition, **2** possesses stereogenic centers on both sides of the TTF framework, thus having a chiral space more pronounced than in **1**. These results point out the importance of the proper selection of the chiral mediators and their interaction with the electrode in order to maximize the chiral induction.

IV. CONCLUSIONS

We have demonstrated the efficiency of two chiral methylated TTF derivatives for electrochemical chiral enantio-discrimination and for chirality induced spin selectivity through spin dependent electrochemistry measurements. The chiral precursors are suitable for the functionalization of gold and nickel surfaces which show very good stability in a wide range of potential. Excellent enantio-recognition was achieved with both Au/TTF platforms towards N,N-dimethyl-1-ferrocenylethylamine, with potential differences between the two enantiomers of 90 – 150 mV, while the recognition of L-Dopa is more effective with compound **2**. The CISS effect is clearly more robust for the latter as well, with average spin polarization values of ±15%, very likely thanks to the more chiral environment created at the interface between the chiral TTF and the nickel surface and thus correlating with the higher ratio of bound *vs* unbound sulfurs as observed by XPS in compound **2** with respect to **1**. These results are a clear proof-of-concept concerning the use of chiral TTFs for electrochemical enantio-discrimination and for the spin polarization and open up numerous perspectives. The electrochemical recognition of redox inactive substrates can be envisaged when taking into account that TTFs are redox active all the more since their redox potentials can be finely tuned by changing the substitution scheme. To comply with the relatively low oxidation potential of metallic Ni, chiral metal bis(dithiolene) complexes can be used as spin polarizers in SDE experiments as they possess much lower oxidation potentials and have accessible reduction stable states.[59,60]

SUPPLEMENTARY MATERIAL

Bulk electrochemistry measurements for **1** and **2**, XPS details and surface area estimation for **1** and **2**.

ACKNOWLEDGMENTS

C.F. gratefully thanks financial support from Dipartimento di Ingegneria “Enzo Ferrari” (DIEF), UniMORE, FARD 2021 - linea di azione di tipo 3: “Materiali chirali per batterie al litio e celle a combustibile” and from Consorzio Interuniversitario Nazionale per la Scienza e Tecnologia dei Materiali (INSTM), fondi triennali: “INSTM21MOFONTANESI”. This work was supported in France by the CNRS, the University of Angers and the French National Agency for Research (ANR)

project SECRETS (ANR PRC 20-CE06-0023-01). Financial support from the French Ministry of Foreign Affairs and University of Angers through an Eiffel scholarship for A.B. is also acknowledged. The authors warmly acknowledge Prof. Ron Naaman (Weizmann Institute of Science, Israel) for fruitful discussions.

AUTHOR DECLARATIONS

Conflict of Interest

The authors have no conflicts to disclose.

Author contributions

Andrea Stefani: Formal analysis (equal); Investigation (equal); Methodology (equal). **Alexandra Bogdan**: Synthesis & characterization (equal). **Flavia Pop**: Synthesis & characterization (lead); Formal analysis (equal). **Francesco Tassinari**: Investigation (equal); Methodology (equal). **Luca Pasquali**: Formal analysis (equal). **Claudio Fontanesi**: Conceptualization (equal); Formal analysis (equal); Funding acquisition (equal); Project administration (equal); Supervision (equal); Writing - original draft (equal); Writing - review & editing (equal). **Narcis Avarvari**: Conceptualization (equal); Funding acquisition (equal); Project administration (equal); Supervision (equal); Writing - original draft (equal); Writing - review & editing (equal).

DATA AVAILABILITY

The data that support the findings of this study are available within the article and its supplementary material.

REFERENCES

[1] R. Naaman, Y. Paltiel, and D. H. Waldeck, Nature Rev. Chem. **3**, 250–260 (2019).

[2] K. Michaeli, N. Kantor-Uriel, R. Naaman, and D. H. Waldeck. Chem. Soc. Rev. **45**, 6478–6487 (2016).

[3] R. Naaman, Y. Paltiel, and D. H. Waldeck, J. Phys. Chem. Lett. **11**, 3660–3666 (2020).

[4] A. Chiesa, A. Privitera, E. Macaluso, M. Mannini, R. Bittl, R. Naaman, M. R. Wasielewski, R. Sessoli, and S. Carretta, Adv. Mater. 2300472 (2023).

[5] T. S. Metzger, S. Mishra, B. P. Bloom, N. Goren, A. Neubauer, G. Shmul, J. Wei, S. Yochelis, F. Tassinari, C. Fontanesi, D. H. Waldeck, Y. Paltiel, and R. Naaman, Angew. Chem. Int. Ed. **59**, 1653–1658 (2020).

[6] K. Banerjee-Ghosh, O. Ben Dor, F. Tassinari, E. Capua, S. Yochelis, A. Capua, S.-H. Yang, S. S. P. Parkin, S. Sarkar, L. Kronik, L. T. Baczewski, R. Naaman, and Y. Paltiel, Science **360**, 1331–1334 (2018).

[7] W. Mtangi, V. Kiran, C. Fontanesi, and R. Naaman, J. Phys. Chem. Lett. **6**, 4916–4922 (2015).

[8] W. Zhang, K. Banerjee-Ghosh, F. Tassinari, and Ron Naaman, ACS Energy Lett. **3**, 2308–2313 (2018).

[9] Y. Liang, K. Banjac, K. Martin, N. Zigon, S. Lee, N. Vanthuyne, F. A. Garcés-Pineda, J. R. Galán-Mascarós, X. Hu, N. Avarvari, and M. Lingenfelder, Nat. Commun. **13**, 3356 (2022).

[10] B. Göhler, V. Hamelbeck, T. Z. Markus, M. Kettner, G. F. Hanne, Z. Vager, R. Naaman, and H. Zacharias, Science **331**, 894–897 (2011).

[11] R. Naaman, Y. Paltiel, and D. H. Waldeck, Acc. Chem. Res. **53**, 2659–2667 (2020).

[12] H. Lu, Z. V. Vardeny, and M. C. Beard, Nature Rev. Chem. **6**, 470–485 (2022).

[13] R. Nakajima, D. Hirobe, G. Kawaguchi, Y. Nabei, T. Sato, T. Narushima, H. Okamoto, and H. M. Yamamoto, Nature **613**, 479–486 (2023).

[14] M. Kettner, V. V. Maslyuk, D. Nürenberg, J. Seibel, R. Gutierrez, G. Cuniberti, K.-H. Ernst, and H. Zacharias, J. Phys. Chem. Lett. **9**, 2025–2030 (2018).

[15] V. Kiran, S. P. Mathew, S. R. Cohen, I. Hernández Delgado, J. Lacour, and R. Naaman, Adv. Mater. **28**, 1957–1962 (2016).

[16] P. C. Mondal, C. Fontanesi, D. H. Waldeck, and R. Naaman, Acc. Chem. Res. **49**, 2560–2568 (2016).

[17] C. Fontanesi, Curr. Opin. Electrochem. **7**, 36–41 (2018).

[18] A. Kumar, P. C. Mondal, and C. Fontanesi, Magnetochemistry **4**, 36 (2018).

[19] D. Mishra, T. Z. Markus, R. Naaman, M. Kettner, B. Göhler, H. Zacharias, N. Friedman, M. Sheves, and C. Fontanesi, Proc. Natl. Acad. Sci. **110**, 14872–14876 (2013).

[20] M. Kettner, B. Gohler, H. Zacharias, D. Mishra, V. Kiran, R. Naaman, C. Fontanesi, D. H. Waldeck, S. Sek, J. Pawlowski, J. Juhaniewicz, J. Phys. Chem. C **119**, 14542–14547 (2015).

[21] N. Bangruwa, P. k. Bhartiya, and D. Mishra, Sens. Actuators B: Chem. **382**, 133447 (2023).

[22] P. C. Mondal, N. Kantor-Uriel, S. P. Mathew, F. Tassinari, C. Fontanesi, and R. Naaman, Adv. Mater. **27**, 1924–1927 (2015).

[23] P. C. Mondal, C. Fontanesi, D. H. Waldeck, and R. Naaman, ACS Nano **9**, 3377–3384 (2015).

[24] S. Arnaboldi, M. Magni, and P. R. Mussini, Curr. Opin. Electrochem. **8**, 60–72 (2018).

[25] S. Grecchi, S. Arnaboldi, S. Rizzo, and P. R. Mussini, Curr. Opin. Electrochem. **30**, 100810 (2021).

[26] F. Sannicolò, S. Arnaboldi, T. Benincori, V. Bonometti, R. Cirilli, L. Dunsch, W. Kutner, G. Longhi, P. R. Mussini, M. Panigati, M. Pierini, and S. Rizzo, Angew. Chem. Int. Ed. **53**, 2623–2627 (2014).

[27] N. Avarvari, and J. D. Wallis, J. Mater. Chem. **19**, 4061–4076 (2009).

[28] F. Pop, N. Zigon, and N. Avarvari, Chem. Rev. **119**, 8435–8478 (2019).

[29] F. Pop, P. Auban-Senzier, E. Canadell, G. L. J. A. Rikken, and N. Avarvari, Nat. Commun. **5**, 3757 (2014).

[30] C. Réthoré, N. Avarvari, E. Canadell, P. Auban-Senzier, and M. Fourmigué, J. Am. Chem. Soc. **127**, 5748–5749 (2005).

[31] A. M. Madalan, C. Réthoré, M. Fourmigué, E. Canadell, E. B. Lopes, M. Almeida, P. Auban-Senzier, and N. Avarvari, Chem. Eur. J. **16**, 528–537 (2010).

[32] F. Pop, P. Auban-Senzier, E. Canadell, and N. Avarvari, Chem. Commun. **52**, 12438–12441, (2016).

[33] S. Matsumiya, A. Izuoka, T. Sugawara, T. Taruishi, and Y. Kawada, Bull. Chem. Soc. Jpn. **66**, 513–522 (1993).

[34] J. D. Dunitz, A. Karrer, and J. D. Wallis, Helv. Chim. Acta **69**, 69–70 (1986).

[35] S. Yang, F. Pop, C. Melan, A. C. Brooks, L. Martin, P. Horton, P. Auban-Senzier, G. L. J. A. Rikken, N. Avarvari, and J. D. Wallis, CrystEngComm **16**, 3906–3916 (2014).

[36] J. R. Galán-Mascarós, E. Coronado, P. A. Goddard, J. Singleton, A. I. Coldea, J. D. Wallis, S. J. Coles, and A. Alberola, J. Am. Chem. Soc. **132**, 9271–9273 (2010).

[37] F. Pop, S. Laroussi, T. Cauchy, C. J. Gómez-García, J. D. Wallis, and N. Avarvari, Chirality **25**, 466–474 (2013).

[38] F. Pop, C. Mézière, M. Allain, P. Auban-Senzier, N. Tajima, D. Hirobe, H. M. Yamamoto, E. Canadell, and N. Avarvari, J. Mater. Chem. C **9**, 10777–10786 (2021).

[39] J. S. Zambounis, C. W. Mayer, K. Hauenstein, B. Hilti, W. Hofherr, J. Pfeiffer, M. Bürkle, and G. Rihs, Adv. Mater. **4**, 33–35 (1992).

[40] N. Mroweh, C. Mézière, F. Pop, P. Auban-Senzier, P. Alemany, E. Canadell, and N. Avarvari, Adv. Mater. **32**, 2002811 (2020).

[41] E. Gomar-Nadal, G. K. Ramachandran, F. Chen, T. Burgin, C. Rovira, D. B. Amabilino, and S. M. Lindsay, J. Phys. Chem. B **108**, 7213–7218 (2004).

[42] M. Starowicz, B. Stypuła, and J. Banaś, Electrochem. Commun. **8**, 227–230 (2006).

[43] F. Tassinari, E. Tancini, M. Innocenti, L. Schenetti, and C. Fontanesi, Langmuir **28**, 15505–15512 (2012).

[44] F. Terzi, L. Pasquali, M. Montecchi, S. Nannarone, A. Viinikanoja, T. Ääritalo, M. Salomäki, J. Lukkari, B. P. Doyle, and R. Seeber, J. Phys. Chem. C **115**, 17836–17844 (2011).

[45] E.T. Kang, K.G. Neoh, and K. L. Tan, Phys. Rev. B **44**, 10461–10469 (1991).

[46] A.-S. Duwez, J. Electron Spectrosc. Relat. Phenom. **134**, 97–138 (2004).

[47] L. Pasquali, F. Terzi, M. Montecchi, B.P. Doyle, J. Lukkari, B. Zanfrognini, R. Seeber, and S. Nannarone, J. Electron Spectrosc. Relat. Phenom. **172**, 114–119 (2009).

[48] F. Terzi, R. Seeber, L. Pigani, C. Zanardi, L. Pasquali, S. Nannarone, M. Fabrizio, and S. Daolio, J. Phys. Chem. B **109**, 19397–19402 (2005).

[49] C. Vericat, M.E. Vela, G.A. Benitez, J. A. M. Gago, X. Torrelles, and R. C. Salvarezza, J. Phys.: Condens. Matter **18**, R867–R900 (2006).

[50] G. Liu, J. A. Rodriguez, J. Dvorak, J. Hrbek, and T. Jirsak, Surf. Sci. **505**, 295–307 (2002).

[51] E. Ito, J. Noh, and M. Hara, Surf. Sci. **602**, 3291–3296 (2008).

[52] M. Gazzotti, S. Arnaboldi, S. Grecchi, R. Giovanardi, M. Cannio, L. Pasquali, A. Giacomino, O. Abollino, and C. Fontanesi, Electrochim. Acta **286**, 271–278 (2018).

[53] L. Dong, Y. Zhang, X. Duan, X. Zhu, H. Sun, and J. Xu, Anal. Chem. **89**, 9695–9702 (2017).

[54] S. Grecchi, S. Arnaboldi, M. Korb, R. Cirilli, S. Araneo, V. Guglielmi, G. Tomboni, M. Magni, T. Benincori, H. Lang, and P. R. Mussini, ChemElectroChem **7**, 3429–3438 (2020).

[55] F. Yang, N. Kong, X. A. Conlan, H. Wang, C. J. Barrow, F. Yan, J. Guo, and W. Yang, Electrochim. Acta **237**, 22–28 (2017).

[56] S. Arnaboldi, S. Cauteruccio, S. Grecchi, T. Benincori, M. Marcaccio, A. Orbelli Biroli, G. Longhi, E. Licandro, and P. R. Mussini, Chem. Sci. **10**, 1539–1548 (2019).

[57] S. Fireman-Shoresh, I. Turyan, D. Mandler, D. Avnir, and S. Marx, Langmuir **21**, 7842–7847 (2005).

[58] F. Pop, M. Allain, P. Auban-Senzier, J. Martínez-Lillo, F. Lloret, M. Julve, E. Canadell, and N. Avarvari, Eur. J. Inorg. Chem. 3855–3862 (2014).

[59] F. Pop, and N. Avarvari, Coord. Chem. Rev. **346**, 20–31 **(**2017)

[60] A. Abhervé, N. Mroweh, T. Cauchy, F. Pop, H. Cui, R. Kato, N. Vanthuyne, P. Alemany, E. Canadell, and N. Avarvari, J. Mater. Chem. C **9**, 4119–4140 **(**2021).